J. Creech
V. Divino
W. Patterson
P. J. Zalesky

TherOx, Inc.,
2400 Michelson Dr.,
Irvine, CA 92612

C. E. Brennen
California Institute of Technology,
MC 104-44,
Pasadena, CA 91125

Injection of Highly Supersaturated Oxygen Solutions Without Nucleation

It is possible to inject highly supersaturated aqueous solutions of gas through a small capillary into an aqueous environment without the formation of significant gas bubbles. Such a technique has considerable potential therapeutic value in the treatment, for example, of heart attacks and strokes. The present paper is the second in a series (see Brereton et al. [1]) investigating the basic phenomenon behind this surprising effect. Recent experiments clearly demonstrate that the nucleation, when it does occur, results from heterogeneous nucleation on the interior surface of the distal end of the capillary. This paper describes the effects of the treatment of this interior surface on the nucleation processes and the results of high speed video observations of the phenomena. A heterogeneous nucleation model is presented which is in accord with the experimental observations. [DOI: 10.1115/1.1519558]

1 Introduction

This paper describes a strategy for the rapid delivery of large quantities of dissolved oxygen to the bloodstream without the formation of oxygen gas bubbles. The potential method benefits of a successful strategy of this kind are substantial and multi-faceted. Deprivation of oxygen even for brief periods of time such as occur during heart attacks or strokes results in cell damage or death—and is the primary cause of permanent physiological damage during these events. Consequently rapid therapeutic oxygen delivery systems could substantially enhance the treatment, for example, of acute myocardial infarction or acute cerebral stroke. It may also find application in a broad range of other medical treatments.

The strategy discussed here has been described previously (Brereton et al. [1]). It involves the preparation of a highly concentrated solution of oxygen in an aqueous solution under very high pressure and the injection of this liquid into the bloodstream through a small capillary tube or tubes. The innovation is the ability to do this in a way that avoids the formation of significant or measurable gaseous oxygen bubbles either inside the capillary or in the highly supersaturated jet that emerges from the tube. This requires two techniques. First the avoidance of nucleation within the capillary over the distal length, l, for which the liquid pressure is below the saturated pressure for the particular oxygen concentration being deployed. And, second, the avoidance of nucleation within the emerging jet. The jet mixes with the surrounding liquid and thus becomes rapidly diluted. If this mixing time is less than the time required for bubbles to grow to observable or significant size then the objective has been achieved. Experiments and analyses of both aspects of the device are described below.

Two basic strategies facilitate success. The first of these is to prepare and treat the interior surface of the capillary in a way that minimizes the occurrence of nucleation sites. The second of the strategies is that of high fluid velocity. Inside the capillary tube this leads to a large longitudinal pressure gradient which implies a short distal length of tube for which the fluid pressure is below the saturation pressure. Minimizing the interior surface area below the saturation pressure minimizes the chance of a nucleation site being activated. However, this paper shows that there is an important upper limit to the velocity for transition to turbulent flow within the capillary tends to promote nucleation. A second benefit of high fluid velocity is that it maximizes the rate of mixing in the jet flow external to the capillary (where turbulence is inconsequential). By using these two strategies it is possible to prepare capillary tubes that can deliver highly concentrated solutions of oxygen without the formation of gaseous bubbles and to do so in such a way that a large fraction of the capillaries are successful in this objective. However, given the uncertainties naturally associated with the occurrence of micron and sub-micron nucleation sites on the interior surface it is inevitable that some of the capillaries will happen to have one or more nucleation sites close enough to the distal end to produce bubbles. A well-regulated testing procedure is necessary to eliminate these defective capillaries. However, the fact that this testing procedure can achieve acceptable success rate is one of the most remarkable and promising aspects of this research.

2 Nucleation Sites

Reviews of nucleation of bubbles in liquids may be found in references such as Skripov [2] or Brennen [3]. In aqueous solutions at normal temperatures, it has been well established that nucleation begins with small, micron-sized bubbles which may be floating freely in the liquid or contained within a crevice of the solid surface that contains the liquid, a process known as heterogeneous nucleation. This is distinct from homogeneous nucleation which refers to the formation of bubbles in the body of a pure liquid as a result of thermodynamic fluctuations. The fact that heterogeneous nucleation dominates in aqueous liquids at normal temperatures, is simply a reflection of the fact that an applied tension will activate far more heterogeneous sites than homogeneous sites.

Heterogeneous nucleation sites include not only the surface of the containing vessel or tube but also the surface of small particles suspended in the liquid. The general term used for such processes is heterogeneous nucleation. Freely floating bubbles or particles with bubbles in crevices will be referred to as free-stream nuclei or sites; sites on the interior containing wall (in this case of the capillary tube) will be referred to as surface nucleation sites. Sometimes, free-stream nuclei dominate as is the case in many cavitating flows (see, for example, Brennen [3]). On the other hand, surface nuclei dominate in pool boiling (see, for example, Griffith and Wallis [4]) because the surface temperature is higher than that of the bulk liquid.

In the context of the present devices, Brereton et al. [1] theoretically explored the possibility of homogeneous nucleation. Subsequent experiments such as those described herein clearly suggested that heterogeneous rather than homogeneous nucleation

Contributed by the Bioengineering Division for publication in the JOURNAL OF BIOMECHANICAL ENGINEERING. Manuscript received Jul. 2001; revised manuscript received Jun. 2002. Associate Editor: J. B. Grotberg.

 Copyright © 2002 by ASME

was dominant. Specifically, it became clear that treatment of the interior surface of the capillary tubes had such a radical effect on the nucleation phenomenon that surface nucleation had to be the dominant phenomenon (see below). The current paper describes those and other experimental observations and presents an analysis of the mechanics of the process which allows evaluation of the parametric variations.

3 Tension Distribution in the Capillary

A key feature of the device and the experiments is the pressure difference or "tension" which motivates nucleation in the distal end of the capillary (internal diameter, d). The tension, $p_{ssat}-p$, is defined as the difference between saturation pressure, p_{ssat}, and the local liquid pressure, p, in the capillary. Under flowing conditions this increases linearly with distance, x, along the tube from zero at the critical location where $p=p_{ssat}$ (called the "saturation location") to $p_{ssat}-p_e$, at the distal end of the capillary, p_e being the ambient pressure at the capillary exit. Since most of the capillary tube flows considered here have Reynolds numbers, Re_t (defined as $\rho_l Vd/\mu$ where V is the volumetric mean velocity of the flow and ρ_l and μ are the liquid density and dynamic viscosity) that cause the flow to be in the laminar regime, the pressure gradient dp/dx within the tube is given by

$$-\frac{dp}{dx}=\frac{32\mu V}{d^2} \tag{1}$$

It follows that the distance, l, from the saturation location, $x=0$, to the end of the capillary, $x=l$, is given by

$$l=\frac{(p_{ssat}-p_e)d^2}{32\mu V} \tag{2}$$

By way of an example, note that in a 100 μm tube at a velocity of 4 m/s and an exit tension of 5 MPa (a typical Brereton et al. [1] data point) the length l is 0.39 m.

4 Surface Nucleation Model—Bubble Growth

To model surface nucleation, we visualize that the interior surface of the distal end of the capillary tube has at least one flaw, crack or crevice that acts as a nucleation site. A bubble grows attached to this site due to diffusion of gas from the liquid into the bubble. When it reaches some critical size, the forces due to the flow around the bubble exceed the surface tension forces holding the bubble in place. The bubble then breaks off and is convected downstream and out of the capillary. A whole series of bubbles is produced by a single site with a frequency that we explore below. There may be just one or two such nucleation sites; alternatively the interior surface may be populated by many nucleation sites.

The key to understanding this process is to recognize that rather than being the precise size of the crevice, the nucleation site size is characterized by R_i because it begins to produce growing, visible bubbles when the tension exceeds the restraining surface tension pressure, $2S/R_i$ (where S is the surface tension). Therefore, given the tension variation described by Eq. (1) only those sites larger than a critical size, $R_{ic}(x)$, will be activated (produce bubbles) at the location, x, where

$$R_{ic}(x)=\frac{Sd^2}{16\mu Vx}=\frac{2S}{(p_{ssat}-p_e)(x/l)} \tag{3}$$

and only those nucleation sites larger than $Sd^2/16\mu Vl=2S/(p_{ssat}-p_e)$ get activated anywhere within the capillary. A few numbers provide guidance on the magnitude of R_{ic} in the present context. For a $d=100$ μm capillary tube at $V=4$ m/s and $(p_{ssat}-p_e)=5$ MPa the values of R_{ic} at $x/l=0.25$, 0.5, and 0.75 are, respectively, 0.112 μm, 0.056 μm, and 0.028 μm. These are very small nucleation sites. Some may be too small to produce exit bubbles of observable size. Another possibility is that there are just a few (maybe just one) large sites which produce bubbles at such a rapid rate that they dominate the observations. We return to these possibilities later.

The next step in developing the model is to estimate the rate of growth of the bubble attached to a nucleation site. Mass transfer of gas into the bubble occurs in the region downstream of the saturation location because the mass fraction of gas in the liquid, c_∞, is greater than that on the surface of the bubble, c_s. The former is clearly given by $c_\infty=p_{ssat}/H$ where H is Henry's Law constant. On the other c_s will be given by $c_s=(p+2S/R)/H$. (This assumes that the bubble is in dynamic equilibrium at all times and therefore that the gas pressure in the bubble is equal to the local liquid pressure plus the surface tension contribution; it can readily be shown that the kind of dynamic growth effects which lead to the Rayleigh-Plesset equation for cavitating bubble growth (Brennen [3]) are negligible in the present context and therefore this assumption is valid). In summary, then, the mass fraction decrement, $c_\infty-c_s$, driving gas into the bubble is given by $(p_{ssat}-p-2S/R)/H$. Clearly this varies with location, increasing from zero at $x=x_i=Sd^2/16\mu VR$ to a maximum of $(p_{ssat}-p_e=2S/R)/H$ at the exit from the capillary. For simplicity, the term $2S/R$ in this expression is neglected in what follows.

The mechanism for mass transfer could be molecular diffusion alone or it could be enhanced by the convective effects of the flow around the bubble. To assess these mechanisms, we evaluate the Peclet number, VR/D, where D is the mass diffusivity of the dissolved gas in the liquid. Since typical values of V are of the order of 4 m/s and D for gases in water is close to 2×10^{-9} m^2/s (more accurately the mass diffusivities, D, of O_2 and CO_2 in water are 2.07×10^{-9} m^2/s and 1.75×10^{-9} m^2/s, respectively (Burkhard and Van Liew [5]) it follows that, if the attached bubble is of any significant size (say greater than 0.1 μm), then the Peclet number is much greater than unity and the mass transfer is dominated by convection. To synthesize this, we consider that there is a thin mass transfer boundary layer around the attached bubble (radius, R) which, using a conventional boundary layer analysis, achieves a thickness of order $(RD/V)^{1/2}$ before separating from the bubble. Evaluating the deficit of mass of gas in this layer whose mass fraction of gas would be somewhere between c_∞ and c_s, we can then estimate the mass flow rate of gas into the bubble which that deficit implies. An order of magnitude estimate would be

$$\rho_l R^{3/2}(DV)^{1/2}(c_\infty-c_s) \tag{4}$$

and since this must be equal to the rate of increase of mass of gas in the bubble this leads to the differential equation

$$\frac{dR}{dt}=C^*\frac{\rho_l}{\rho_g}R^{-1/2}(DV)^{1/2}(c_\infty-c_s) \tag{5}$$

where C^* is some constant of order unity. Solving this leads to an expression for the growth of the bubble radius, $R(t)$, as a function of time, t:

$$R=C^{**}(DV)^{1/3}\left\{\frac{\rho_l(p_{ssat}-p)t}{H\rho_g}\right\}^{2/3} \tag{6}$$

where C^{**} is another constant of order unity. This bubble growth phase will end when the bubble detaches from the site, an event we explore next.

5 Surface Nucleation Model—Bubble Departure

When the surface-nucleated bubble becomes large enough, it will be torn off the surface by the drag inflicted by the flow. The next stop is to evaluate the size of the departing bubble, R_d. A rough estimate of the magnitude of the surface tension force acting at the line of contact between the bubble and the surface and holding the bubble to the surface would be $2\pi R_i S$. The drag force opposing this and tending to tear the bubble away from the nucleation site is more complex. First it depends on the Reynolds num-

ber, $Re_b = 2\rho_l V_b R/\mu$, of the flow around the bubble where V_b denotes the typical fluid velocity impinging on the bubble. Since the bubble is in the shear flow on the interior surface of the capillary, an appropriate expression for V_b is VR/d.

When the bubble Reynolds number, Re_b, is small, the drag can be approximated by $6\pi\mu V_b R$. In which case the bubble leaves the surface when it has achieved a radius, R_d, of

$$R_d = \left\{ \frac{R_i S d}{3\mu V} \right\}^{1/2} \tag{7}$$

On the other hand when the Reynolds number, Re_b, exceeds about 100 it is more accurate to use a high Reynolds number expression for the drag with a drag coefficient of about 0.5. Then the appropriate expression for the drag would be $1/4\pi R^2 \rho_l V_b^2$ which leads to

$$R_d = \left\{ \frac{8 R_i S d^2}{\rho_l V^2} \right\}^{1/4} \tag{8}$$

Next we examine whether Eqs. (7) or (8) is relevant to the present circumstance. To do so consider typical nucleation sites with $R_i = 1$ μm and $R_i = 0.1$ μm and a velocity, $V = 4$ m/s. Expressions (7) and (8) then both yield $R_d = 24$ μm for $R_i = 1$ μm. For $R_i = 0.1$ μm they give $R_d = 8$ μm and $R_d = 14$ μm, respectively. The corresponding bubble Reynolds numbers range from 8 to 40 and are therefore in an awkward intermediate range. However, we choose the high Reynolds number expression since it yields a reasonable approximation in this range.

We should also note that some of the above bubble sizes are a significant fraction of the diameter of the tube. The resulting blockage effect will lead to larger drag coefficients and cause a reduction in R_d below the estimate in Eq. (8). The net effect in this parametric range of operation is that the departure radius, R_d, asymptotes to some fraction of the diameter of the tube, d.

When Eq. (8) is combined with Eq. (6) it completes the model of the bubble growth and departure from a nucleation site at a location, x, in the capillary. For example, the frequency, f, of bubble production from a site close to the distal end of the capillary (where $p \approx p_e$ and $p_g \approx p_e$) would be given by

$$f = C R_d^{-3/2} (DV)^{1/2} \left\{ \frac{\rho_l (p_{ssat} - p_e)}{H \rho_e} \right\} \tag{9}$$

where C is some constant of order unity.

6 Bubble Growth in Jet

Whatever their source, the bubbles emerging from the capillary will continue to grow as they are carried along in the unconfined jet. The range of flow rates and capillary diameters being used in the experiments happens to span the critical Reynolds numbers for the jets so even though the flow inside the capillaries may be laminar, the emerging jet can be laminar or turbulent. The conditions experienced by the bubbles in these two cases are quite different and we should consider how they lead to the eventual bubble size and void fraction. First we review some of the basic mixing properties of an axisymmetric jet (see Schlichting [6]) emerging from a tube into a similar liquid. Setting aside some of the details which need not be considered here, both laminar and turbulent jets grow linearly with distance, x, from the exit while the typical jet velocity, V_x, is inversely proportional to that distance. Thus

$$\frac{V_x}{V} = \left\{ 1 + \lambda \frac{x}{d} \right\}^{-1} \tag{10}$$

and the ratio of the volume flow rate in the jet at distance x to the volume flow rate emerging from the tube is therefore $1 + \lambda(x/d)$. Then, if we consider that the entrained liquid is thoroughly mixed with the original jet liquid (more true in a turbulent jet than in a laminar one) it follows that the mass fraction of dissolved oxygen, c_x, that surrounds a bubble travelling in the jet should be given by

$$\frac{c_x}{c_\infty} = \left\{ 1 + \lambda \frac{x}{d} \right\}^{-1} = \frac{p_{xsat}}{p_{ssat}} \tag{11}$$

Clearly when the local saturated pressure, p_{xsat}, falls below the local ambient pressure, p_e, the oxygen bubble being carried along by the jet will cease to grow. The critical distance, x_c, at which this happens is then given by

$$\frac{x_c}{d} = \frac{(p_{ssat} - p_e)}{\lambda p_e} \tag{12}$$

It is also useful to estimate the total bubble growth from the exit to this location where growth ceases. For this purpose we follow a model of growth by convection similar to that described in Section 4 except that we will denote the convective fluid velocity around the bubble by V_c and try to visualize how that might be evaluated in a laminar or a turbulent jet. In either case, using V_c in place of V, c_x in place of c_∞ and $V_x dR/dx$ in place of dR/dt in Eq. (8), we obtain a differential equation for $R(x)$ as a function of x. Taking V_c as independent of x as a first approximation, the differential equation can be integrated to obtain

$$R(x)^{3/2} - R(0)^{3/2} = \frac{3\rho_l C d (DV_c)^{1/2}}{4\rho_e V} \left\{ 2(c_\infty - c_s)\frac{x}{d} - \lambda c_s \frac{x^2}{d^2} \right\} \tag{13}$$

and therefore the maximum or final bubble size, $R(x_c)$, is given by

$$R(x_c)^{3/2} = R(0)^{3/2} + \frac{3\rho_l C d (DV_c)^{1/2} (p_{ssat} - p_e)^2}{4\rho_e V \lambda H p_e} \tag{14}$$

These results all depend upon the parameter, λ, which is directly related to the jet spreading angle, θ, by $\lambda = 2\tan(\theta/2)$. In the case of a laminar jet $\lambda = 16\mu/Vd$ and this would pertain for values of the Reynolds number, Vd/μ, greater than unity but less than the value at which transition occurs in the jet. Above this value the jet becomes turbulent a short distance downstream of the exit and reasonable values consistent from previous observations (for example, Papanicolaou and List [7]) are $\theta = 25°$ and $\lambda = 0.44$ (see also Section 8).

7 Experimental Equipment

A set of experiments was conducted to investigate the onset of nucleation in highly super-saturated liquid jets emerging from small capillary tubes. The results reported below show clearly that the condition of the interior surface near the exit from the capillary is a critical factor in the resulting behavior. Consequently the material of the capillary, its roughness, coating(s) and preparation were important. The experiments reported here focused on drawn silica capillaries with internal diameters ranging from 75 μm to 325 μm though results are also described for some polymer (PEEK) capillaries.

The smoothness and cleanliness of the interior and posterior surfaces of the capillaries were important in minimizing the possibilities for nucleation. Thus the silica capillaries were cleaved in such a way that the end appeared very rectangular and flat under microscopic examination. Some which showed significant deformity or irregularity were discarded. On the other hand the PEEK capillaries were sliced with sharp razor while being held in a jig. Photographs of the distal ends of typical capillaries are included in Fig. 1; note that the PEEK appears rougher than the silica.

The interior surface of the silica capillaries were prepared in various ways. Some of the capillaries were coated with benzalkonium heparin (BKH for short), a biocompatible treatment designed for medical devices. After pre-treating the surface with

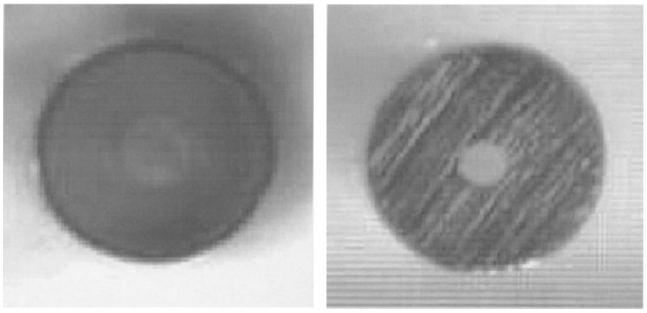

Fig. 1 Photographs of the distal ends of typical capillaries formed from silica (left) and PEEK (right)

ethanol, the BKH was deposited on the interior surface of the capillary by dissolving it in a 10% solution in isopropyl alcohol (aka 2-propanol) and then evaporating the alcohol.

The experiments utilized various concentrations of oxygen and carbon dioxide in distilled water (filtered down to 2 μm) at normal temperatures. These solutions were prepared under high pressure so that the saturated pressures of oxygen employed varied from 0.17 to 6.41 MPa though the focus was on the higher levels above 1.38 MPa. Experiments were also conducted with carbon dioxide because its much higher solubility would provide information on the importance of that parameter; CO_2 saturated pressures ranging from 0.41 to 3.37 MPa were employed. Note that the Henry's Law constants (defined as the partial pressure of gas divided by the saturated mass fraction of gas in the liquid under that partial pressure) for oxygen and carbon dioxide in water at 25°C are 2590 MPa and 70 MPa respectively (Schmidt and List [8]). For later reference we also note that the same properties for ethanol rather than water are 249 MPa and 17 MPa respectively (Dack [9]). Note that these solubilities in ethanol are an order of magnitude larger than the solubilities in water.

The experiments themselves are simple. Using a special high pressure delivery system (US Patent 5,893,838) in which the flow rate could be carefully adjusted, the highly concentrated solutions were pumped through the capillary tube whose distal end was submerged in a large beaker of water (large so that dissolved gas build up did not result in nucleation in the host liquid). Careful visual observation of the emerging jet determined whether or not nucleation was occurring. Sometimes a microscope was used to aid these observations.

8 Jet Visualization

Early in the testing it was discovered that the nature of the flow within the capillary tube (whether it was laminar or turbulent) could have a significant impact on whether or not nucleation occurred. The usual Reynolds numbers for transition in a tube range from 2000 to 4000 with rougher tubes having lower values. In the current experiments this transition could be readily investigated by using alcohol rather than water as the host liquid in the receiving beaker. The emerging jet could then be readily visualized due to the difference in the refractive index of water and alcohol.

At low Reynolds numbers when the flow within the capillary was laminar, the emerging jet was smooth and grew very slowly with distance from the end of the capillary as exemplified by the left hand photograph in Fig. 2. Such was the case for many capillaries (particularly the smooth silica tubes) even at Reynolds numbers just below the critical. This observation may be strange to those expecting instability and transition to occur just downstream of the exit. Such would indeed be the case for a jet emerging from a nozzle with a relatively uniform velocity profile and therefore a strong shear layer at the jet surface. However, these emerging velocity profiles are quite parabolic and the shear layers are much less unstable. Other capillaries (particularly the rougher PEEK capillaries) did show shear layer transitions though typically 10 to 15 jet diameters from the exit. Thus, in all cases the distance from the exit to the beginning of transition was much longer than occurs with uniform velocity profile jets.

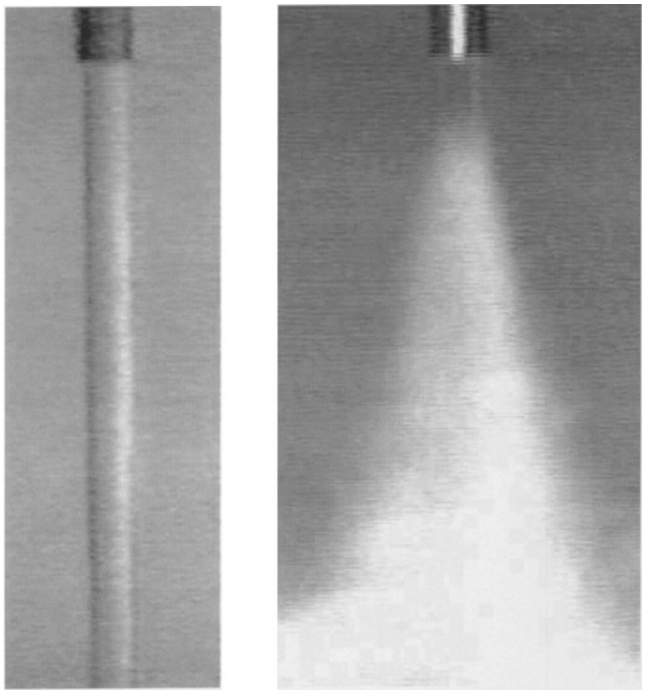

Fig. 2 Frames from a normal video showing typical laminar (left) and turbulent jets (right) emerging from a 325 μm capillary

Irrespective of the evolution of the laminar jet, it was clear that above some Reynolds number, the flow within the capillary began to undergo transition and emerge from the exit as a turbulent jet. Such is the case with the right hand photograph in Fig. 2. With many capillaries (but not all) this transitional process would begin at transitional Reynolds numbers with a condition in which the appearance of the jet would flip-flop back and forth between the photographs in Fig. 2, the flip-flop being completed in less time than the interval between the frames of the normal speed video (in other words less than 0.02 s). Moreover, each state could last for several frames or for as little as a single frame. It was exceedingly rare to capture the switching process in a single frame and those frames were difficult to interpret. As the flow rate was increased, the turbulent jet configuration occurred for a greater and greater fraction of the frames until the laminar configuration completely ceased to appear. We note that the frequency of flip-flopping, F, when converted to a reduced frequency, Fd/V yielded values of the order of 10^{-4}.

This switching was also observed with the PEEK tubes for which the emerging laminar jet would undergo transition 10 to 15 jet diameters from the exit. The video recording would flip-flop back and forth between two turbulent jet configurations, one of which had a laminar jet section. We note that the range of flow rates over which switching occurred was smaller than for the smooth silica tubes.

In the case of the PEEK tubes (which are hydraulically rougher than the silica tubes), the internal flow transition occurred, as expected, at lower flow rates and Reynolds numbers than in the silica capillaries as can be seen in Table I below. The following data demonstrates that all the transitional Reynolds numbers were in a range close to 2000.

As described in Section 6, another useful piece of data is the spreading angle, θ, for the turbulent jets; typically this was close to 25° as exemplified by Fig. 2 (right).

Table 1 Capillary tubes.

Tube	d (μm)	Material	Transitional Values	
			V (m/s)	Re_t
B2	325	Silica	6.2	2020
C2	250	Silica	8.8	2210
H1	250	PEEK	6.8	1700
E2	100	PEEK	17–26	1700–2600

9 Nucleation Observations

It is convenient to begin this presentation of the nucleation results by describing a series of observations with a typical capillary. Normally, the capillaries began the tests in a dry state. Some (but not all) had been coated with BKH, then dried and stored. The experiments were then begun by connecting one end of the capillary to the high pressure supply system and submerging the other end in a large beaker of distilled water. A flush of distilled water was run through the capillary in order to purge the system of trapped gas bubbles. The supply was then switched to the highly concentrated solution of O_2 or CO_2. The initial supply pressure had previously been adjusted to produce the desired flow rate. If nucleation was going to occur it would happen almost instantaneously and persist as long as the flow continued and the operating conditions remained unchanged. When nucleation did not occur, that state would remain indefinitely; experiments were continued for as long as the supply lasted (tens of minutes) to confirm the permanence of the nucleation-free operation. Sometimes nucleation could be initiated by increasing the flow rate until the internal flow became turbulent (turbulence seemed to promote nucleation). In such cases, the nucleation would persist even when the flow rate was decreased so that the flow became laminar again.

In many of the cases when nucleation occurred, the capillary was subsequently disconnected from the supply and several ml of ethanol forced through it with a syringe (for convenience we refer to this as ''ethanolization''). Then the capillary would be reconnected to the supply and the nucleation test repeated. In the large majority of the cases in which this was done, the nucleation was completely suppressed—and the capillary would run indefinitely without nucleation.

This effect of ethanolization was a most remarkable and dramatic phenomenon. It was also permanent; nucleation would not occur no matter how long the experiment ran. However, when a nucleation-free flow caused by ethanol was stopped, the capillary dried out and then reinstalled, the capillary would revert to its nucleation behavior prior to ethanolization. Thus, once nucleation sites became active again or were exposed to air, the benefit caused by the ethanol would disappear. However, another ethanolization would reinstitute the nucleation-free effect. Experiments were performed through a half-dozen such cycles to confirm the reversibility of the phenomenon.

While any explanation of this remarkable effect must be somewhat tentative, it appears that, even underwater, the ethanol preferentially wets the solid surface and dislodges the tiny gas bubbles (nuclei) in the crevices that cause nucleation. Clearly this is a consequence of ethanol preferentially wetting the solid surface. In addition, as pointed out in Section 7, the solubility of all gases in ethanol is much greater than in water so the ethanol may also be eliminating nucleation sites by dissolving the gas. Once removed or at least reduced below some stabilized size, the nucleation site is not reactivated even after the ethanol has all been washed away by the flow. Hence the permeance of the effect. Only drying out the surface and recharging the crevice with air reactivates the site.

We note that ethanol worked with the PEEK as well as the silica capillaries. Moreover, other surface treatments had a somewhat similar effect. First the BKH coating on the silica clearly inhibited nucleation since coated capillaries had a superior performance to those without the coating. However, when a BKH coated capillary failed, subsequent ethanolization had the same restorative effect described above. Indeed the ethanolized, BKH-coated capillaries were the most remarkable performers of all.

Isopropyl alcohol was also tried as an alternative to ethanol; it was less effective, working in some cases but not in others. Finally, we note that a few nucleating capillaries could not be made non-nucleating by ethanolization. However, when these were examined through the microscope, they were found to have large deformities or cracks near the distal end.

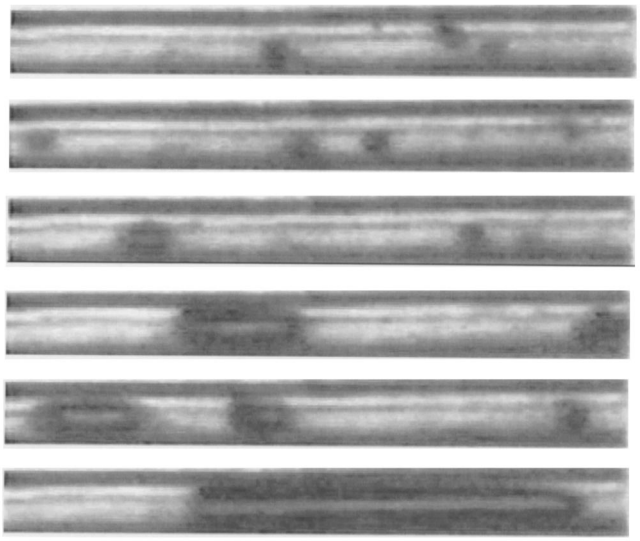

Fig. 3 Six examples of high-speed video frames showing bubbles about to exit a particular 250 μm capillary. The distal end of the capillary is on the right.

10 High Speed Video Observations

High-speed videos were taken of the bubbles both in the jet and in the capillary in order to further document the phenomenon. A Redlake Imaging Motionscope 8000S video camera with a Toyo Optics TV Zoom Lens was used for this purpose. At 8000 fps framing rate it was possible to discern individual bubbles both within the capillary and in the jet. Figures 3 and 4 are examples of single frames from that video.

Figure 3 presents 6 examples of frames that include bubbles passing through the distal end of a 250 μm BKH-coated silica capillary with a 3.45 MPa O_2 solution flowing at 3.4 m/s. In these frames the distal end of the capillary is on the left and the bubbles appear as black shadows through the transparent capillary wall.

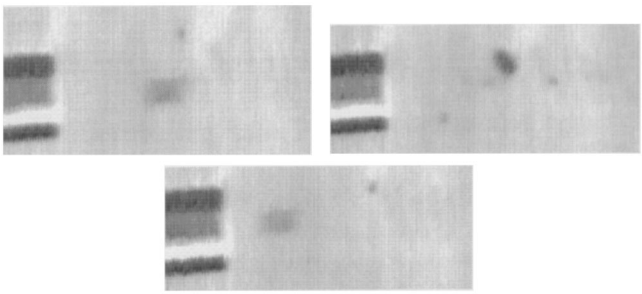

Fig. 4 Three examples of high-speed video frames showing the faint images of bubbles that have just emerged from a 325 μm capillary

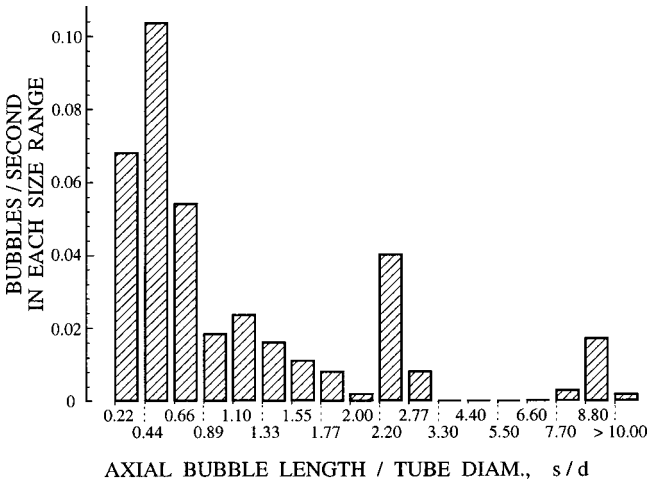

Fig. 5 Typical histogram of the axial bubble length, *s*, divided by the tube diameter, *d*. Note that bubbles with $s/d<1$ are roughly spherical while those with $s/d>1$ are tube-filling slugs. This particular histogram is for a BKH-coated silica capillary with diameter 250 μm operating with a 3.45 MPa O_2 solution at a velocity of 3.4 m/s.

The four upper frames show smaller bubbles, one of which is of the 2.5*d* variety. The lowest frame shows one of the 10*d* bubbles discussed below.

Figure 4 shows the faint images of bubbles that have just emerged from a 325 μm BKH-coated silica capillary with a 3.45 MPa O_2 solution flowing at 4 m/s. These appeared to break up rapidly in the turbulent jet so that they generate quite indistinct images in the video.

Analysis of the high speed videos revealed rather different bubble production patterns in the 250 μm and 325 μm capillaries and changing patterns with changing flow rate.

In describing these patterns we choose to begin by detailing the observations of the bubbles emerging from a particular 250 μm capillary when the flow rate is such as to produce a fluid velocity of 3.4 m/s (Fig. 3). The smallest bubbles that could be observed had various globular shapes with diameters of about 0.2*d*. The frame-to-frame analysis suggested that these were being distorted by the flow; sometimes it appeared as though this distortion led to bubble fission since the bubble actually appeared to be a cloud of smaller bubbles. Bubbles smaller than 0.1*d* may have been present in the intervening liquid but would have been difficult to resolve. However, they did not seem to be present in significant numbers or aggregate volume since the intervening liquid appeared to be clear and transparent. The largest bubbles which were observed exiting the capillary were large tube-filling slugs about 10*d* long as illustrated in Fig. 3.

There are several possible explanations for these large slug bubbles which we explore below. However, there are some other observations that should be discussed first. A histogram of the bubble axial length (see, for example, Fig. 5) shows that virtually all the larger slug bubbles lie within quite narrow size ranges. For example, there appear to be a regular series of 10*d* bubbles and virtually no bubbles in the range $3d-8d$. Another, less distinct peak occurred at 2.3*d*. Second, the data showed that, after the passage of a large, 10*d* slug, there was always an extended period when no bubbles exited the capillary. In the specific case under discussion, the bubble free interval following the expulsion of a large 10*d* slug averaged 0.0018 s in comparison with the typical interval between exiting bubbles of 0.0004 s.

Using these observations we can construct a likely course of events in the capillary. The large bubble-free interval following 10*d* slugs suggests that there is a single nucleation site quite far from the exit whose detaching bubbles regularly sweep clean all the other sites on their way to the exit. Since the subsequent bubble-free interval is 0.0018 s and the velocity is 3.4 m/s this implies that this particular nucleation site is at least 0.0061 m from the exit.

Next we observe that the rate of production of 10*d* bubbles is about 160 per second. In comparison, Eq. (9) predicts a rate of 88 per second from a single site provided we take C in that equation to be unity. A value of $C=2$ is definitely within the expected uncertainty. Finally, since the total number of bubbles exiting the capillary is about 2500 per second, we can estimate (using $C=2$) that the number of active nucleation sites in this particular capillary is 14.

But why are the large slugs 10*d* in length? This size could be the result of one or both of the following growth mechanisms: (a) the bubble detaching from the most upstream site with a diameter of about 1*d* might collect additional gas by agglomeration with the bubbles growing at the other 14 sites and/or (b) the bubble simply expands due to the decrease in the prevailing pressure between the nucleation site and the capillary exit. However, the latter mechanism is negligible since the pressure change between the estimated site location and the exit is only about a tenth of an atmosphere. It therefore seems likely that the bubble mostly grows to 10*d* in length by adding roughly 1*d* at each of the 14 sites it passes on the way to the capillary exit.

We now examine how the pattern of events changed when the flow velocity in this particular capillary was decreased from 3.4 m/s to 1.7 m/s. At this lower velocity, the dominant large slugs were 28*d* in length rather than 10*d*. Again there was a bubble-free interval following each slug but this was now 0.0035*s* (compared with the average intra-bubble spacing of 0.0009*s*). However, at 1.7 m/s, this bubble-free gap again implies a nucleation site 0.006 m upstream, in good agreement with the observation at 3.4 m/s. The production rate for the large 28*d* slugs was 115 per second and this again compares favorably with the prediction of equation 9 with $C=2$ which is 124 per second. The total event rate is 903 per second and this would suggest 8 active nucleation sites, somewhat smaller than the 14 estimated from the 3.4 m/s data.

In contrast to the 250 μm capillary, the bubbles exiting the 325 μm capillary all appeared to have axial lengths in the range 0.5*d* to 1.2*d*, with virtually no larger slugs. Perhaps there are no large slugs because there is no dominant nucleation site far enough upstream but it is otherwise hard to be sure of the reason for the difference. The typical diameter of the bubbles exiting the tube decreased with increasing flow rate, declining from about 1.0*d* at a velocity of 3 m/s to about 0.5*d* at a velocity of 6 m/d. When the bubbles exit the capillary, they appear to be substantially distorted by the flow and may even be broken into fragments. Though the typical size changed with increasing flow rate, the rate of efflux of bubbles seemed to be independent of velocity, being about 1100 bubbles per second at all three speeds. At the three speeds examined, the tension length, l, is 3.8 m, 2.8 m, and 1.9 m for velocities of 3 m/s, 4 m/s, and 6 m/s, respectively. Thus, while the frequency of bubble production from a single site may increase with velocity in the manner suggested by Eq. (9), the tension length and therefore the number of active sites may be declining so as to keep the bubble production rate constant. Using Eq. (9) with $C=2$, the rate of 1100 bubbles per second suggests that there are a total of about 8 active nucleation sites in this 325 μm capillary.

We conclude that the observations of the bubbles emerging from the capillaries are consistent with the heterogeneous nucleation model presented earlier in the paper. However, each capillary has its own particular number of nucleation sites which is not capable of prediction by any current theory. It is however notable that the estimated number of nucleation sites in each of the closely-examined capillaries was a small or modest number (14, 8, and 8). Certainly small enough so that one could visualize their elimination by ethanolization.

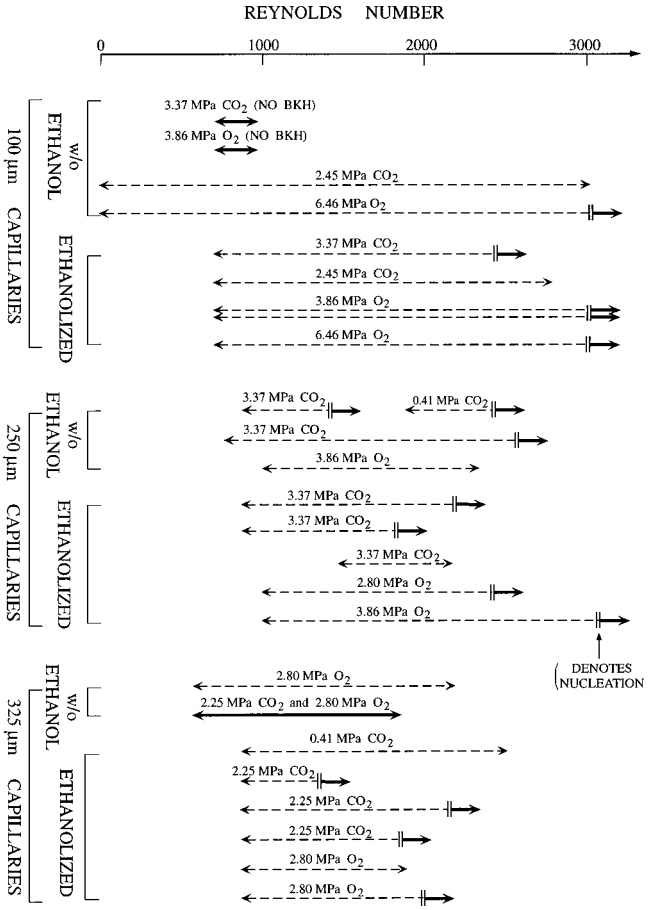

Fig. 6 Chart showing the results of tests carried out to investigate nucleation caused by the onset of turbulent flow within the capillary. Horizontal lines show nucleating (solid lines) and non-nucleating (dashed lines) Reynolds number ranges for a number of different capillaries (with and without ethanolization) operated with various aqueous solutions of O_2 and CO_2 (saturation pressures shown). Onset of nucleation as the flow rate and Reynolds number was increased is shown by the two short vertical lines.

11 Effect of Flow Rate

With each of the capillaries, the flow rate was varied in order to determine whether nucleation preferentially occurred over one particular range of flow rates or, possibly, over some particular Reynolds number range. One speculation was that since the length, *l*, decreases with increasing velocity, the larger surface area under tension at lower flow rates would make nucleation more likely at those low flow rates. However, this was never observed experimentally perhaps because the range of flow rates over which experiments could be performed was quite limited.

As mentioned earlier, the primary effect of flow rate occurred when the flow rate was increased to that value at which the internal flow became turbulent. Much of the evidence for this conclusion is displayed graphically in Fig. 6, a chart that displays the results of tests carried out to investigate nucleation caused by the onset of turbulent flow within the capillary. Included are the observed nucleating (solid lines) and non-nucleating (dashed lines) Reynolds number ranges of different silica capillaries operated with various aqueous solutions of O_2 and CO_2. With two exceptions, all capillaries were initially coated with BKH; results with and without ethanolization are also shown. Onset of nucleation as the flow rate (Reynolds number) was increased is shown by the two short vertical lines.

The purpose of the chart is to demonstrate that, in these increasing flow rate tests, most of the critical Reynolds numbers at which nucleation occurred are contained within the range 2000–3000, in other words the range at which the internal flow transitions from laminar to turbulent. It thus appears that turbulence promotes nucleation. This could be the result of momentary low pressures induced at the wall by the turbulence but this is clearly speculative.

12 Effect of Gas Concentration

As mentioned previously, tests were conducted not only with different gas concentrations but also with both O_2 and CO_2. Since ethanolization effectively re-initialized a given capillary, it was possible to conduct repeatable tests on a particular capillary with both O_2 and CO_2 as well as with different concentrations of both gases.

In the vast majority of cases, the high concentrations of O_2 and CO_2 behaved identically in terms of whether or not nucleation occurred in a particular capillary. The most noticeable difference was that a nucleating flow with CO_2 had a higher concentration of gas (or void fraction) than the flow with O_2. The obvious reason for this is that the mass fraction of the CO_2 solutions was typically much greater than that of the O_2 solutions. This supports the notion that the dominant factor that determines whether or not macroscopic bubbles are observed is the presence or absence of nucleation sites rather than a critical concentration gradient of dissolved gas. Parenthetically we note that one consequence of the similarity of behavior in O_2 and CO_2 is that it is simpler and more foolproof to test capillaries with CO_2 since the nucleation is more dramatic.

An effort was also made to ascertain experimentally whether there was a trend with gas concentration. Collections of ten 325 μm silica tubes freshly coated with BKH and of ten and five 100 μm PEEK capillaries were tested in solutions of O_2 with saturation pressures ranging from 1.93 MPa to 4.76 MPa. Though some evidence of an increasing probability of nucleation with increasing gas content was observed, the scatter in the data did not permit definite conclusions.

13 Concluding Remarks

The experiments described in this paper confirm a remarkable phenomenon in which highly-supersaturated aqueous solutions of gas may be injected through a small capillary into an aqueous environment without the formation of significant and/or measurable gas bubbles. This technique has considerable potential therapeutic value in many medical treatments and could also prove valuable in other technologies. By comparing the experiments with a theoretical model which treats (1) the potential formation and growth of bubbles at nucleation sites inside the capillary at its distal end (2) the detachment and ejection of such bubbles from the capillary and (3) potential growth of the bubbles in the emerging jet, it is shown that the laboratory observations are consistent with such a heterogeneous nucleation model. Of particular note is the estimate that, in the successful silica capillaries, the number of potential nucleation sites is of the order of ten.

It is also clear that the treatment of the interior surface of the capillary is critical to the success or failure of the objective since it can effectively eliminate the last remaining nucleation sites, though perhaps only when they are small in number. Several treatments are remarkably effective in this regard. One simple technique that was deployed in the laboratory was to flush the capillary with ethanol after it had already been filled with an aqueous medium. Apparently, the ethanol strips out or dissolves the nucleation sites and causes them to become non-functional. This is an entirely reversible procedure; allowing the capillary to dry out re-establishes the functioning nucleation sites; and another ''ethanolization'' will eliminate them again. A medical device coating which has a similar though less dramatic effect is a benzalkonium heparin (BKH).

Because of the sensitivity of the phenomenon to surface treatment, each capillary is quite unique and it is therefore difficult to

establish the dependence of the nucleation threshold on the fundamental flow variables, namely the capillary diameter, the flow velocity and the gas concentration. For example, it is difficult to duplicate the simple relation between the maximum nucleation-free gas concentration and the tube diameter presented by Brereton et al. [1]. However, apart from the sensitivity to surface treatment, the present study did establish that when the flow (a) in the capillary or (b) in the emerging jet transitions from a laminar to a turbulent state this can trigger nucleation, presumably because of the greater mass transfer which occurs in the turbulent regime.

Acknowledgments

The authors are very grateful for the help given by Gustavo Joseph during the high speed video observations.

Nomenclature

c_∞ = Mass fraction of gas in liquid [-]
c_s = Mass fraction of gas in liquid at bubble surface [-]
c_x = Local mass fraction of gas in jet [-]
C, C^*, C^{**} = Constants of order unity [-]
d = Capillary internal diameter [μm]
D = Mass diffusivity of gas in liquid [m^2/s]
f = Frequency of bubble production from a single site [s^{-1}]
F = Jet flip-flopping frequency [s^{-1}]
H = Henry's Law constant, p_{ssat}/c_∞ [MPa]
l = Distal capillary length for which $p < p_{ssat}$ [m]
p = Pressure in capillary [MPa]
p_e = Capillary exit pressure [MPa]
p_{ssat} = Saturation pressure of the dissolved gas [MPa]
R = Bubble size [μm]
R_d = Bubble size at departure [μm]
R_i = Nucleation site size [μm]
R_{ic} = Critical nucleation site size [μm]
Re_b = Bubble Reynolds Number, $2\rho_l V_b R/\mu$ [-]
Re_t = Capillary Reynolds Number, $\rho_l V d/\mu$ [-]
s = Bubble axial length [μm]
S = Surface tension [kg/s^2]
t = Time [s]
V = Volumetric velocity inside capillary [m/s]
V_b = Typical liquid velocity impinging on bubble [m/s]
V_c = Convective liquid velocity around bubble [m/s]
V_x = Jet velocity [m/s]
x = Axial distance along capillary [m]
x_c = Critical axial distance in jet [m]
λ = Jet spreading parameter, 2 tan $\theta/2$ [-]
μ = Liquid dynamic viscosity [kg/ms]
ν = Liquid kinematic viscosity [m^2/s]
ρ_l = Liquid density [kg/m^3]
θ = Jet spreading angle [-]

References

[1] Brereton, G. J., Crilly, R. J., and Spears, J. R., 1998, "Nucleation in Small Capillary Tubes," Chem. Phys., **230**, p. 253.
[2] Skripov, V. P., 1974, *Metastable Liquids*, John Wiley and Sons.
[3] Brennen, C. E., 1995, "Cavitation and Bubble Dynamics," Oxford University Press.
[4] Griffith, P., and Wallis, G. D., 1960, "The Role of Surface Conditions in Nucleate Boiling," Chem. Eng. Prog., Symp. Ser., **56**, pp. 30–49.
[5] Burkhard, M. E., and Van Liew, H. D., 1994, "Simulation of Exchanges of Multiple Gases in Bubbles in the Body," Respiration Physiology, **95**, pp. 131–145.
[6] Schlichting, H., 1960, "Boundary Layer Theory (4th ed.)," McGraw-Hill Book Company.
[7] Pananicolaou, P. N., and List, E. J., 1988, "Investigation of Round Vertical Turbulent Buoyant Jets," J. Fluid Mech., **195**, p. 341.
[8] Schmidt, A. X., and List, H. L., 1962, "Material and Energy Balances," Prentice-Hall.
[9] Dack, M. R. J. (editor), 1975–76, "Solutions and Solubilities," in "Techniques of Chemistry," 8, John Wiley and Sons.